membranes

*Article*

# N-Doped HNT/$TiO_2$ Nanocomposite by Electrospinning for Acetaminophen Degradation

**Mahmoud Abid [1,2], Elissa Makhoul [1], Fida Tanos [1], Igor Iatsunskyi [3], Emerson Coy [3], Geoffroy Lesage [1], Marc Cretin [1], David Cornu [1,*], Abdesslem Ben Haj Amara [1,†] and Mikhael Bechelany [1,*,†]**

1 Institut Européen des Membranes, IEM, UMR 5635, Univ. Montpellier, ENSCM, CNRS, 34730 Montpellier, France
2 Laboratory of Resources, Materials & Ecosystem (RME), Faculty of Sciences of Bizerte, University of Carthage, Zarzouna 7021, Tunisia
3 NanoBioMedical Centre, Adam Mickiewicz University, Wszechnicy Piastowskiej 3, 61-614 Poznan, Poland
* Correspondence: david.cornu@umontpellier.fr (D.C.); mikhael.bechelany@umontpellier.fr (M.B.)
† These authors contributed equally to this work.

**Abstract:** In this study, we combined electrospinning of a large amount of halloysite (HNT, 95%) with nitriding to produce N-HNT-$TiO_2$ composite nanofibers (N-H95T5 hereafter) to be used for acetaminophen (ACT) photodegradation. Investigation of the morphological and structural properties of the obtained materials did not highlight any significant difference in their morphological features and confirmed that nitrogen was evenly distributed in the samples. Photocatalytic tests under visible light showed that acetaminophen photodegraded faster in the presence of samples with nitrogen (N-H95T5) than without (H95T5 nanofibers). Moreover, the N-H95T5 nanocomposite photocatalytic activity did not change after repeated utilization (five cycles). The addition of scavengers during photocatalytic tests showed the key implication of $OH^{\bullet -}$, $O_2^{\bullet -}$ and $h^+$ radicals in acetaminophen degradation. These results indicated that N–H95T5 composite nanofibers could be considered a cheap multifunctional material for photodegradation and could open new prospects for preparing tunable photocatalysts.

**Keywords:** halloysite nanotubes; $TiO_2$ nanofibers; electrospinning; nitriding; photocatalysis; acetaminophen



**Citation:** Abid, M.; Makhoul, E.; Tanos, F.; Iatsunskyi, I.; Coy, E.; Lesage, G.; Cretin, M.; Cornu, D.; Ben Haj Amara, A.; Bechelany, M. N-Doped HNT/$TiO_2$ Nanocomposite by Electrospinning for Acetaminophen Degradation. *Membranes* **2023**, *13*, 204. https://doi.org/10.3390/membranes13020204

Academic Editor: Mazeyar Parvinzadeh Gashti

Received: 19 December 2022
Revised: 13 January 2023
Accepted: 3 February 2023
Published: 7 February 2023



## 1. Introduction

Water pollution is a major problem leading to health and environmental issues [1]. With proper water treatment, such as by heterogeneous photocatalysis, it is possible to reduce water pollution by degrading pollutants [2–4]. $TiO_2$ is the most used material in water purification systems because of its low cost, low toxicity, relatively high efficiency, and high chemical and thermal stability [5,6]. However, two of its major drawbacks are the limited recovery after water treatment and the rapid recombination of the photogenerated charges [7]. Therefore, substantial research has been conducted to optimize $TiO_2$ photocatalytic activity [8,9]. For instance, doping and surface modification have been studied to improve the utilization of sunlight. $TiO_2$ has been doped using metal ions (e.g., Pd [10,11], Ag [12,13], Pt [10]), non-metal ions (e.g., B, N, Cu, Ni), and semi-conductors (e.g., BN, ZnO, CuO) [14–17] to enhance its photocatalytic activity.

According to the atomic orbital theory, nitrogen doping increases the amount of nitrogen in the first energy level N 1s and in the O 2p orbital of $TiO_2$. This allows for increasing the number of electrons in the conduction band and the number of holes in the valence band and limiting the in situ recombination of electron-hole pairs after excitation with visible light [18]. In nitrogen-doped $TiO_2$, the semiconductor bandgap is reduced (thus facilitating the photocatalyst activation), the light response range is broadened, and the number of photogenerated carriers is increased [19,20]. Recently, Asahi et al. showed that $TiO_2$ optical absorbance into the visible light region is enhanced after nitrogen doping [21]. Nitrogen-doped $TiO_2$ (N-$TiO_2$) can be prepared using different methods,

such as hydrothermal synthesis and calcination in the presence of $NH_3$ [22] and by post-synthesis nitriding at 500 °C. In the last study, the authors highlighted the improved activity of N-$TiO_2$ for acetone oxidation under visible light [23]. Moreover, nitrogen doping by treatment with ammonium nitrate in water at pH 5.87 strongly increased N-$TiO_2$-mediated degradation of 2,4-dichlorophenol following exposure to visible light [24]. These findings indicate that nitrogen doping improves $TiO_2$ photocatalytic activity by promoting hydroxyl and superoxide radical production.

Recently, Abid et al. prepared $TiO_2$-based composite nanofibers with 95% halloysite (H95T5) and demonstrated that these nanocomposites degraded 91% of acetaminophen under visible light irradiation in 360 min [25]. Here, we explored the preparation and photocatalytic performance of nitrogen-doped H95T5 (N-H95T5) composite nanofibers. We found that these new nitrogen-doped nanocomposites eliminated more than 95% of acetaminophen in the presence of visible light in only 270 min. We then used high-performance liquid chromatography (HPLC) and toxicity assays to determine the intermediates and reaction products generated during the photocatalytic process and their toxicity and found out that the percentage of bacterial luminescence inhibition by ACT decreased to 6% after 24 h using N-H95T5 compared to 52% with H95T5 [25]. We identified the main reactive species explaining acetaminophen degradation using scavenger tests.

## 2. Materials and Methods

### *2.1. Materials*

All chemicals listed in Table 1 were used without further purification.

**Table 1.** Materials used in this work, suppliers, mass fraction purity, and CAS number.

| Material | Supplier/Source | Purity | CAS Number |
|---|---|---|---|
| Halloysite (HNT) | Tamra (Nefza District, NW Tunisia) | - | - |
| Titanium tetraisopropoxide (TTIP) | Sigma–Aldrich | 97% | 546-68-9 |
| Polyvinyl pyrrolidone (PVP) | Sigma–Aldrich | Mw = 1,300,000 | 9003-39-8 |
| Sodium chloride | Sigma–Aldrich | ≥99% | 7647-14-5 |
| Silver nitrate | Sigma–Aldrich | ≥99% | 7761-88-8 |
| Acetaminophen (ACT) | Sigma–Aldrich | ≥99% | 103-90-2 |
| 2-propanol (IPA) | Sigma–Aldrich | 99.9%, | 67-63-0 |
| p-benzoquinone (BQ) | Sigma–Aldrich | ≥99.5%, | 106-51-4 |
| Ethylenediaminetetraacetic acid (EDTA) | Sigma–Aldrich | 99.995%, | 60-00-4 |
| Acetic acid | VWR chemicals | - | 64-19-7 |
| Ethanol | VWR chemicals | ≥99.8%, | 64-17-5 |
| Deionized water | Milli-Q® Academic | >18.2 MΩ | |

### *2.2. Preparation of N-H95T5 Composite Nanofibers*

N-H95T5 samples were prepared by electrospinning and nitriding following previously described protocols [25,26]. Polyvinylpyrrolidone solution was prepared by dissolving PVP powder into ethanol solution. Then, halloysite was added to $TiO_2$ prepared by hydrolyzing titanium tetraisopropoxide into a mixture of acetic acid and ethanol. The precursor mixture was stirred for 1 h at room temperature and electrospun. The obtained nanofibers were left exposed to air overnight to hydrolyze followed by heating at 400 °C for 4 h in air and sintering in a tubular furnace at 500 °C for 1 h (under nitrogen atmosphere).

### *2.3. Structural Characterizations*

The samples' structures, phase, and crystallinity were determined by scanning electron microscopy (SEM; Hitachi S-4800) and transmission electron microscopy (TEM; JEOL ARM 200F).

Surface and micropore areas were described using the Brunauer-Emmett-Teller (BET) method, with different data points and relative pressures (P/Po) from 0 to 1. Their structural and crystallinity properties, elemental composition, and oxidation states were analyzed by X-ray diffraction (XRD; PANAlytical Xpert-PRO diffractometer equipped with an X'celerator detector using Ni-filtered Cu-radiation), Fourier-transform infrared spectroscopy (FT-IR) was recorded with the NEXUS instrument, equipped with an attenuated total reflection accessory in the frequency range of 400–4000 $cm^{-1}$, Raman (Horiba Xplora, 532 nm), and X-ray photoelectron spectroscopy (XPS) with an ESCALAB 250 spectrometer (Thermo Electron; excitation source: Al K$\alpha$ monochromatic source, 1486.6 eV), respectively.

### *2.4. Electrochemical Activity*

Electrochemical impedance spectroscopy was performed as previously published [25,27].

### *2.5. Photocatalytic Activity*

For photocatalytic activity testing, acetaminophen degradation in the presence of different samples and of visible light was carried out as in our previous work [25] and quantified with Equation (1) [28].

$$\text{Degradation efficiency (\%)} = [(C_0 - C)/C_0] \times 100, \quad (1)$$

where $C_0$ and C are the pollutant concentrations before and after irradiation.

Acetaminophen was chosen for these tests because it is consumed in all countries of the world, has been detected in water samples from different origins, and is very stable in water [14,17,25,29–32].

### *2.6. Kinetics*

Acetaminophen photocatalytic degradation kinetic data were fitted using a pseudo-first-order kinetic model [33]:

$$\ln (C_0/C) = K_{app}\, t, \quad (2)$$

where $C_0$ is the initial concentration, C is the concentration at time t, and $K_{app}$ is the apparent rate constant.

### *2.7. Micro-Toxicity Tests*

To assess the toxicity of the solution during acetaminophen photodegradation, microtoxicity tests were carried out using the bioluminescent marine bacterium *Vibrio fischeri* as described in [25].

## 3. Results and Discussion

### *3.1. H95T5 and N-H95T5 Morphology and Structure*

H95T5 and N-H95T5 morphological features were characterized by SEM. In both samples, nanofibers were uniform, continuous, and randomly oriented (Figure S1a,b). This confirmed that the introduction of nitrogen did not change $TiO_2$ shape, in good agreement with the literature [22,25,34].

Crystallinity analysis of H95T5 and N-H95T5 by XRD showed (Figure S2) the characteristic 001 reflection of HNT (7.18 Å) at 2θ, and $TiO_2$ anatase phase with tetragonal arrangement reflections at nearly 2θ = 25.36, 37.7, 48.06, 54.01, 55.00, 62.49, 68.61, 69.68, and 74.85° ascribed to the (101), (112), (200), (105), (211), (204), (116), (220), and (215) Miller plans, respectively [25]. XRD patterns indicated that the main $TiO_2$ reflection was shifted from the initial position after nitriding. Likewise, no significant difference was found between H95T5 and N-H95T5 by Raman and Fourier-transform infrared spectroscopy (Figure S3).

High-resolution TEM (Figure 1a–c) indicated that N-H95T5 nanofibers had a rough and large surface area with a lattice spacing of 0.350 nm, fully consistent with the distance of the (101) crystalline plane of the $TiO_2$ anatase [25,35,36]. Doping with nitrogen changed neither the morphology of N-H95T5 compared with H95T5 [25] nor the crystal lattice

values (selected area electron diffraction images). In fact, elemental mapping can be used for qualitative (the type of elements) as well as quantitative (the percentage of the concentration of each element of the sample) analysis. In N-H95T5, there are more than four elements. Then, it is recommended to proceed with the quantitative analysis by indicating the concentration of elements by a change in color: from blue (low concentration) to red (high concentration) to green in the middle. Figure 1d–i confirmed the homogenous distribution of nitrogen with T, O, Al, and Si elements.

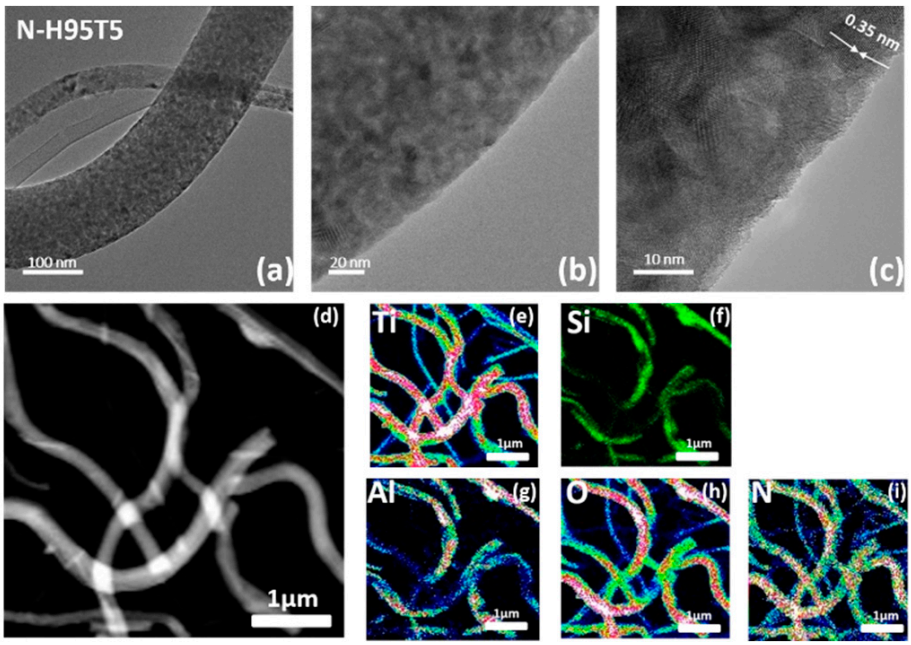


**Figure 1.** TEM images (**a**–**c**) and STEM-EDX chemical mapping of N-H95T5 (**d**–**i**).

This section may be divided by subheadings. It should provide a concise and precise description of the experimental results, their interpretation, as well as the experimental conclusions that can be drawn.

N-H95T5 surface structure and chemical state were investigated by XPS. The survey spectrum of H95T5 and N-H95T5 (Figure 2a) contained the dominant signals of Ti 2p and O 1s and the weak signals of C 1s, Al 2p, and Si 2p. In comparison, nitrogen content can be detected in the nitrogen-treated H95T5 sample. Figure S4 shows the N 1s peak for these samples before and after nitriding. For further analysis of the chemical structure of the N-H95T5 samples, high-resolution spectrum of XPS was used to identify the elements present in the N-H95T5 nanofibers in three areas. The Ti 2p region near 460 eV (Figure 2b), the N 1s region near 400 eV (Figure 2c), and the O 1s region near 530 eV (Figure 2d).

The Ti 2p spectrum (Figure 2b) presented two peaks (458.73 and 464.43 eV: Ti $2p_{3/2}$ and Ti $2p_{1/2}$). After deconvolution of the N 1s peak, only one peak was detected with binding energy at 399.82 eV (Figure 2c). The N 1s binding energy peak was broad, ranging from 396.32 eV to 403.91 eV and centered at 399.82 eV, which was greater than the typical binding energy of 397.2 eV in Ti-N; therefore, Ti-N bonds were excluded and this peak could be assigned to the presence of O-Ti-N linkage [37,38]. In the O 1s spectrum (Figure 2d), the peaks at 529.84 and 531.50 eV were assigned to O-Ti and O-H. respectively. The XPS spectra displayed a third peak that shifted to a higher binding energy (+0.7 eV) after nitriding (Table 2). This bond could be attributed to the Ti-O-N or O-Ti-N bonds mainly on the surface [39,40]. The XPS spectra confirmed nitrogen distribution into H95T5 nanofibers.

Nitrogen is commonly used for BET surface analysis because of its high purity and strong interaction with most solids. Since the interaction between gas and solid phases is generally weak, the surface is cooled with liquid $N_2$ to obtain detectable levels of adsorption. A known amount of nitrogen gas is then gradually released into the sample cell. Relative

pressures less than atmospheric pressure are achieved by creating conditions of partial vacuum. After the adsorption layer is formed, the sample is removed from the nitrogen atmosphere and heated at room temperature to release the adsorbed nitrogen from the material and quantify it. Heating from −200 °C to 25 °C has no great effect on the surface morphology and architecture of N-H95T5 nanofibers. Figure 3 demonstrates that the N-H95T5 exhibited a type IV isotherm and a type H2 hysteresis loop at a lower relative pressure region [41]. The BET method gave specific surface area values of 36.6 $m^2/g$ for H95T5 and 67.85 $m^2/g$ for N-H95T5. This increase was due to nitrogen incorporation in $TiO_2$ nanofibers and should be beneficial for photocatalytic activity by creating more active adsorption sites [42].

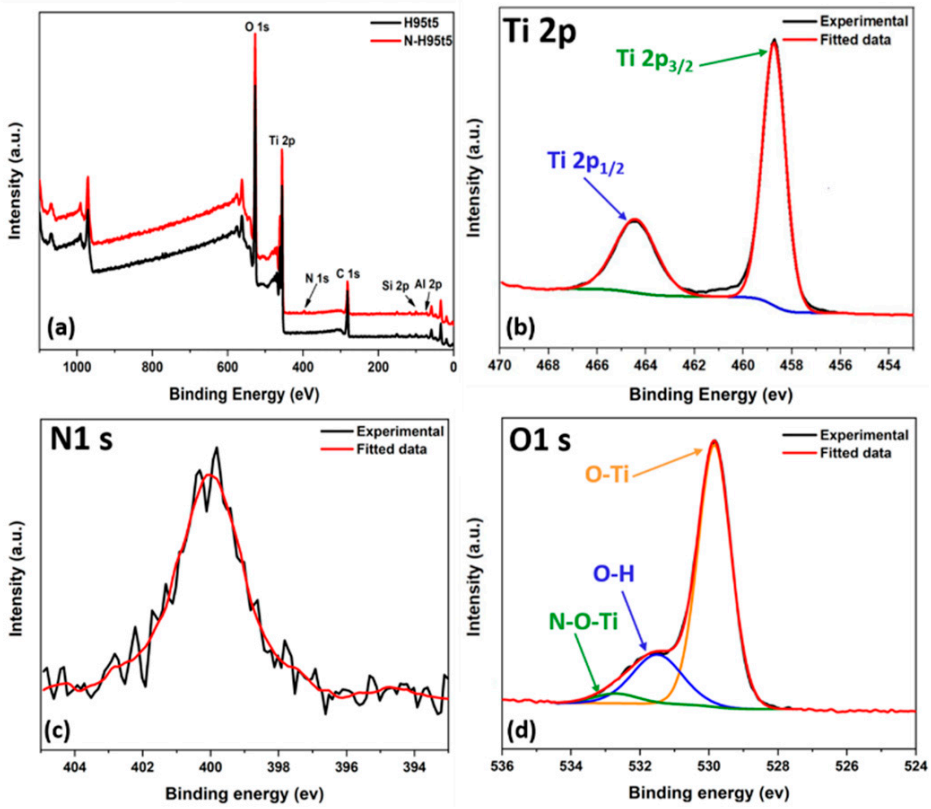


**Figure 2.** Comparison of the X-ray photoelectron spectra of H95T5 and N-H95T5 (**a**) and high-resolution XPS spectra of (**b**) Ti 2p, (**c**) N 1s, and (**d**) O 1s.

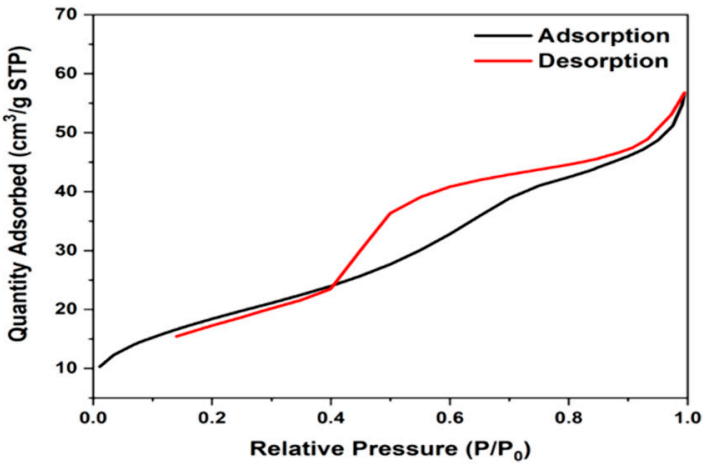


**Figure 3.** Nitrogen adsorption-desorption isotherms of N-H95T5.

**Table 2.** Deconvoluted peaks of O 1s and Ti 2p.

| H95T5 | Position | N-H95T5 | Position |
|---|---|---|---|
| O 1s O-Ti | 529.7 | O 1s N-O-Ti | 529.84 |
| O 1s O-H O=C | 531.1 | O 1s O-H | 531.50 |
| O 1s O-Si O-C | 532.0 | O 1s O-Ti | 532.70 |
| Ti $2p_{3/2}$ $TiO_2$ | 458.5 | Ti $2p_{3/2}$ $TiO_2$ | 458.73 |
| Ti $2p_{1/2}$ $TiO_2$ | 464.2 | Ti $2p_{1/2}$ $TiO_2$ | 464.43 eV |

### *3.2. Electrochemical Activity*

Electrochemical impedance spectroscopy with the previously described model was used to investigate N-H95T5 electrochemical activity [25]. Figure 4a,b show that the impedance arc radius of electrodes in the dark was much bigger than that under visible light irradiation, which indicated that there were few electrons across the electrolyte interfaces in the dark. While under visible light, the arc radius of the N-doped H95T5 electrode was smaller than that of the undoped electrode. This demonstrated that the N-H95T5 displayed greater separation efficiency of photogenerated electron-hole pairs and faster charge transfer than H95T5. It can be seen that the resistance of N-H95t5 decreased by 89% after its exposure to visible light irradiation compared with 85% for H95T5. Charge transfer rate was 10% faster and photogenerated electron-hole separation improved, as indicated by the lower $R_2$ value (1148 Ω for N-H95T5 versus 1280 Ω for H95T5). This indicates that heat treatment with an inert nitrogen atmosphere is a promising way to improve the efficiency of photocatalyst.

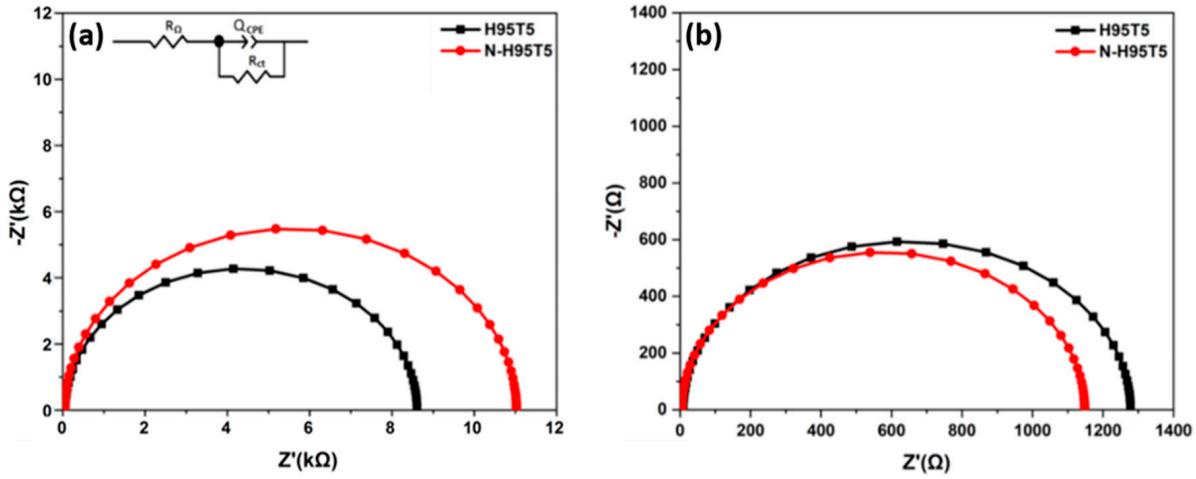


**Figure 4.** Nyquist curves of H95T5 and N-H95T5 in the dark (**a**) and with visible light (**b**). The proposed circuit is shown in the inset.

Then, acetaminophen degradation quantification in the presence of N-H95T5 or H95T5 and visible light for 4.5 h (Figure 5a) showed an increase in photocatalytic efficiency with N-H95T5 at the end of the experiment (83% and 95% of acetaminophen degraded with H95T5 and with N-H95T5, respectively). These data suggest that nitrogen doping increases oxygen vacancies that promote the trapping of photoinduced electrons and that act as a reactive center for photocatalysis [23,43].

Table 3 summarizes the degradation activity of previously studied photocatalysts for organic pollutants in water, highlighting the comparable performance of N-H95T5.

Acetaminophen degradation kinetics was explained by a pseudo first-order reaction (curve linearity and linear coefficient $R^2$~1) (Figure 5b). The lower electron-hole recombination rate explained the enhanced acetaminophen degradation with N-H95T5.

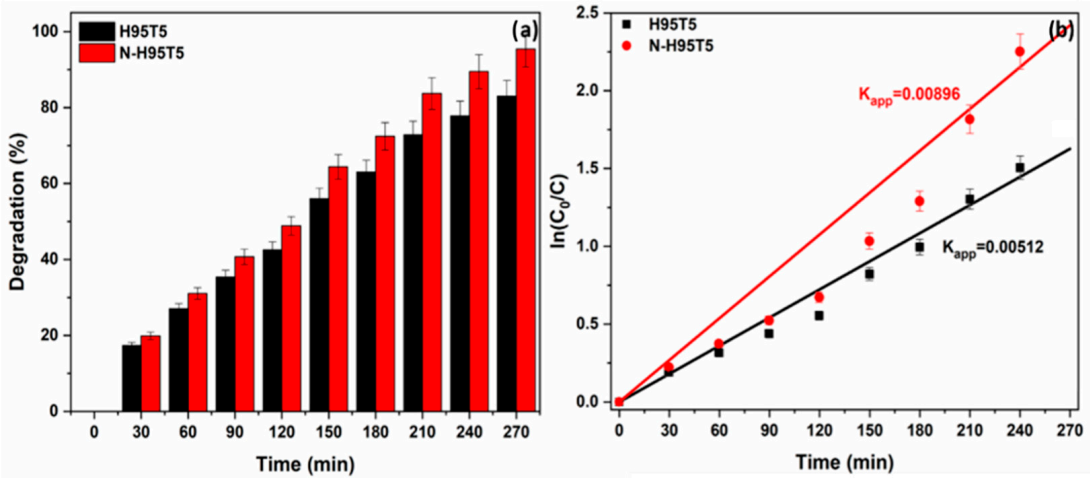


**Figure 5.** Degradation rate of acetaminophen in the presence of H95T5 and N-H95T5 upon exposure to visible light (**a**) and acetaminophen degradation kinetics (**b**). Data are the mean value of three measurements and the relative error is lower than ±5%.

**Table 3.** Photocatalytic activity of different photocatalysts.

| Pollutant (mg/L) | Photocatalyst (g/L) | Synthesis Technique | Visible Light Source | Degradation Efficiency (%) | Degradation Time (min) | Ref. |
|---|---|---|---|---|---|---|
| Acetaminophen (ACT) (10 mg/L) | N-H95T5 (0.5 g/L) | Electrospinning + nitriding | Halogen linear lamp | 95 | 270 | This work |
| ACT (10 mg/L) | H95T5 (0.5 g/L) | Sol-gel + electrospinning | Halogen linear lamp | 91 | 360 | [25] |
| Rhodamine B (10 mg/L) | N-$TiO_2$ (1g/L) | Sol-gel + ammonia treatment | 500 W mercury lamp | 90 | 120 | [22] |
| Gaseous toluene | N–$TiO_2$ | Sol-gel + ammonia atmosphere treatment | 150 W Xe lamp with an IR cutter | 48 | 60 | [21] |
| Rhodamine B (20 mg/L) | N-$TiO_2$ (1g/L) | Microemulsion–hydrothermal method | 1000 W halogen lamp | 96 | 60 | [44] |
| 2,4-dichlorophenol (2,4-DCP) (100 mg/L) | | | | 56 | 300 | |
| Methyl Orange (MO) (20 mg/L) | N-$TiO_2$-400 (0.062 g/L) | Precipitation + ammonium hydroxide | Visible light | 52 | 836 | [45] |
| 2,4-DCP (100 mg/L) | N-$TiO_2$ (1g/L) | Sol-gel+ $NH_4NO_3$/$NH_3$ $H_2O$ | 1000 W halogen lamp | 52 | 300 | [24] |
| ACT (5 mg/L) | N-$TiO_2$-NTs (0.5g/L) | ALD + nitriding | Halogen linear lamp | 98 | 90 | [34] |
| MO (9.8 mg/L) | N-$TiO_2$ (1g/L) | Solid state dispersion + urea | Solar light | 91 | 90 | [46] |
| Methylene Blue (MB) (10 mg/L) | N-$TiO_2$ (1g/L) | Wet chemical method + urea | Visible light | 72 | 180 | [47] |

After the photocatalysis experiment, the photocatalyst was removed by filtration, washed with deionized water several times, and dried at 80 °C for 12 h, then treated for 15 min at 500 °C to remove all impurities and water molecules. Then, the catalyst was analyzed by BET. The BET method gave specific surface area values of 678,512 $m^2$/g for N-H95T5 and 60.8532 $m^2$/g for regenerated N-H95T5. A loss of 11% was found but the obtained value remained higher than raw H95T5.

N-H95T5 reusability was confirmed by monitoring acetaminophen (10 mg/L, pH 7) degradation over five cycles (same conditions as before). After each experiment, N-H95T5 was filtered, washed in water, and dried (100 °C for 12 h). Acetaminophen degradation reached 95.45% in the first run and then was 93.54%, 92.11%, 86.95%, and 83.04% (Figure 6a).

The decrease of 17% after five consecutive cycles could be related to nitrogen loss after each run or to the accumulation of degradation by-products on the catalyst surface that decrease the number of available active sites [48]. Despite this loss of activity after five cycles, N-H95T5 can be considered a promising stable catalyst for industrial applications.

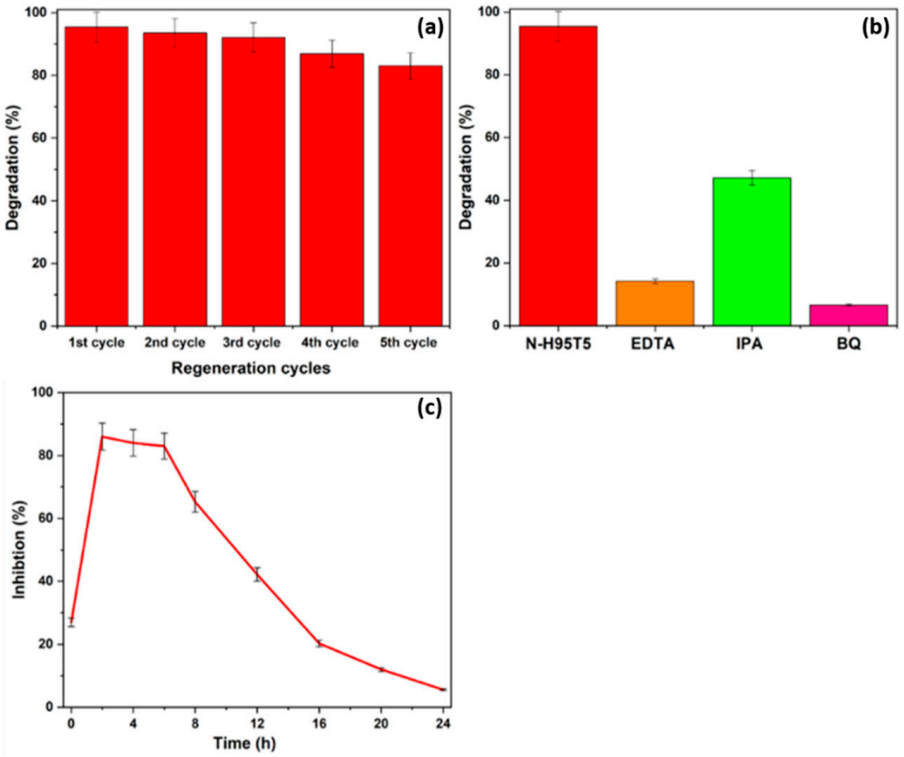


**Figure 6.** N-H95T5 is a stable photocatalyst (**a**). Acetaminophen photodegradation in the presence of N-H95T5 and of the indicated scavengers (**b**). Vibrio fischeri fluorescence inhibition during acetaminophen degradation by N-H95T5 (**c**). IPA, isopropanol; BQ, p-benzoquinone.

Then, acetaminophen degradation assays were performed using the same experimental conditions, but in the presence of N-H95T5 and different scavengers (0.06M [49]) to determine what reactive radicals are implicated in this photocatalytic process [49] (Figure 6b). The addition of isopropanol ($^{\bullet}OH$ scavenger) strongly decreased the acetaminophen degradation rate. The strongest inhibitory effects were obtained with benzoquinone ($O_2^{\bullet -}$ scavenger) and with EDTA ($h^+$ scavenger). Therefore, all three radical types are implicated in acetaminophen photodegradation [17,25].

Lastly, toxicity assays were performed to monitor the formation of harmful by-products during acetaminophen degradation. When *Vibrio fischeri* was incubated with N-H95T5 and acetaminophen, its natural fluorescence was inhibited by 27% after 15 min and up to 86% after 2 h of exposure to visible light to induce acetaminophen degradation (Figure 6c). Fluorescence inhibition progressively decreased: 83% at 6 h, 65% at 8 h, 42% at 12 h, 12% at 20 h, and 6% at 24 h. This indicates that after 24 h, the toxic aromatic by-products generated during acetaminophen photodegradation were transformed into nontoxic compounds [33,50,51].

## 4. Conclusions

This study describes the fabrication of H95T5 and N-H95T5 composite nanofibers by combining electrospinning and nitriding. After doping with nitrogen, no significant difference was found between H95T5 and N-H95T5 by Raman, FT-IR, XRD, and SEM. In addition, nitrogen was homogeneously distributed with T, O, Al, and Si as proved by elemental mapping. In the XPS survey spectrum, Ti 2p and O 1s were the dominant signals, while C 1s, Al 2p, Si 2p, and N 1s were weaker. The charge transfer rate was faster and

electron-hole separation was improved by nitrogen doping. Nitrogen doping also enhanced the catalytic properties of the prepared sample, with a degradation rate of 0.0089 $min^{-1}$. Recyclability tests were promising, as indicated by the loss of only 17% of activity after five cycles. The scavenging experiments revealed that $^{\bullet}OH$, $h^+$ and $O_2^{\bullet-}$ were strongly implicated in acetaminophen photodegradation. Toxicity (i.e., *V. fischeri* fluorescence inhibition) was high in the first 4h of acetaminophen photodegradation in the presence of N-H95T5, due to the generation of aromatic by-products (1,4-benzoquinone, benzoic acid, and benzaldehyde) that were later transformed into nontoxic compounds. This study has confirmed that a cheap photocatalyst with low $TiO_2$ and nitrogen concentrations can be used for the degradation of organic molecules and has opened prospects for mass production and practical applications.

**Supplementary Materials:** The following supporting information can be downloaded at: https://www.mdpi.com/article/10.3390/membranes13020204/s1, Figure S1: SEM micrographs showing H95T5 (a) and N-H95T5 nanocomposite fibers (b); Figure S2: XRD patterns of H95T5 and N-H95T5 nanocomposite fibers; Figure S3: FT-IR spectra (a) and Raman spectra (b) of H95T5 and N-H95T5 nanofibers; Figure S4: XPS survey spectra of H95T5 and N-H95T5 from 420 to 380 ev.

**Author Contributions:** M.A.: methodology, validation, formal analysis, investigation, data curation, writing—original draft, visualization. E.M.: data curation, formal analysis, writing—review and editing. F.T.: data curation, formal analysis, writing—review and editing. I.I.: formal analysis, investigation, resources, writing—review and editing, visualization. E.C.: formal analysis, investigation, resources, writing—review and editing, visualization. G.L.: validation, resources, writing—review and editing, supervision. M.C.: validation, writing—review and editing, funding acquisition. D.C.: validation, writing—review and editing, funding acquisition. A.B.H.A.: conceptualization, resources, writing—review and editing, supervision, funding acquisition. M.B.: conceptualization, resources, writing—review and editing, supervision, project administration, funding acquisition. All authors have read and agreed to the published version of the manuscript.

**Funding:** This work was possible due to the financial support of H2020-MSCA-RISE-2017, 'Novel 1D photonic metal oxide nanostructures for early stage cancer detection' (Project number: 778157). I.I. received funding from the NCN SONATA-BIS program (UMO-2020/38/B/ST5/00176). M.A. thanks the Ministry of Higher Education and Scientific Research of Tunisia for financial support.

**Institutional Review Board Statement:** Not applicable.

**Informed Consent Statement:** Not applicable.

**Data Availability Statement:** Not applicable.

**Conflicts of Interest:** The authors declare no conflict of interest.

## References

1. Bozkir, V. *A Moral Failure: Billions of People with No Access to Clean Drinking Water*; Inter Press Service: Rome, Italy, 2021.
2. Herrmann, J.-M. Heterogeneous Photocatalysis: Fundamentals and Applications to the Removal of Various Types of Aqueous Pollutants. *Catal. Today* **1999**, *53*, 115–129. [CrossRef]
3. Rauf, M.A.; Ashraf, S.S. Fundamental Principles and Application of Heterogeneous Photocatalytic Degradation of Dyes in Solution. *Chem. Eng. J.* **2009**, *151*, 10–18. [CrossRef]
4. Rauf, M.A.; Meetani, M.A.; Khaleel, A.; Ahmed, A. Photocatalytic Degradation of Methylene Blue Using a Mixed Catalyst and Product Analysis by LC/MS. *Chem. Eng. J.* **2010**, *157*, 373–378. [CrossRef]
5. Coy, E.; Siuzdak, K.; Pavlenko, M.; Załęski, K.; Graniel, O.; Ziółek, M.; Balme, S.; Miele, P.; Weber, M.; Bechelany, M.; et al. Enhancing Photocatalytic Performance and Solar Absorption by Schottky Nanodiodes Heterojunctions in Mechanically Resilient Palladium Coated $TiO_2$/Si Nanopillars by Atomic Layer Deposition. *Chem. Eng. J.* **2020**, *392*, 123702. [CrossRef]
6. Moma, J.; Baloyi, J. Modified Titanium Dioxide for Photocatalytic Applications. In *Photocatalysts—Applications and Attributes*; Bahadar Khan, S., Akhtar, K., Eds.; IntechOpen: London, UK, 2019. [CrossRef]
7. Ali, I.; Asim, M.; Khan, T.A. Low Cost Adsorbents for the Removal of Organic Pollutants from Wastewater. *J. Environ. Manag.* **2012**, *113*, 170–183. [CrossRef] [PubMed]
8. Tu, H.; Li, D.; Yi, Y.; Liu, R.; Wu, Y.; Dong, X.; Shi, X.; Deng, H. Incorporation of Rectorite into Porous Polycaprolactone/$TiO_2$ Nanofibrous Mats for Enhancing Photocatalysis Properties towards Organic Dye Pollution. *Compos. Commun.* **2019**, *15*, 58–63. [CrossRef]

9. Wu, H.; Inaba, T.; Wang, Z.-M.; Endo, T. Photocatalytic $TiO_2$@CS-Embedded Cellulose Nanofiber Mixed Matrix Membrane. *Appl. Catal. B Environ.* **2020**, *276*, 119111. [CrossRef]
10. Nasr, O.; Mohamed, O.; Al-Shirbini, A.-S.; Abdel-Wahab, A.-M. Photocatalytic Degradation of Acetaminophen over Ag, Au and Pt Loaded $TiO_2$ Using Solar Light. *J. Photochem. Photobiol. Chem.* **2019**, *374*, 185–193. [CrossRef]
11. Zhu, Y.; Gao, C.; Bai, S.; Chen, S.; Long, R.; Song, L.; Li, Z.; Xiong, Y. Hydriding Pd Cocatalysts: An Approach to Giant Enhancement on Photocatalytic CO2 Reduction into CH4. *Nano Res.* **2017**, *10*, 3396–3406. [CrossRef]
12. Nasr, M.; Soussan, L.; Viter, R.; Eid, C.; Habchi, R.; Miele, P.; Bechelany, M. High Photodegradation and Antibacterial Activity of BN–Ag/$TiO_2$ Composite Nanofibers under Visible Light. *New J. Chem.* **2018**, *42*, 1250–1259. [CrossRef]
13. Khojasteh, H.; Salavati-Niasari, M.; Sangsefidi, F.S. Photocatalytic Evaluation of RGO/$TiO_2$NWs/Pd-Ag Nanocomposite as an Improved Catalyst for Efficient Dye Degradation. *J. Alloys Compd.* **2018**, *746*, 611–618. [CrossRef]
14. Nasr, M.; Viter, R.; Eid, C.; Habchi, R.; Miele, P.; Bechelany, M. Enhanced Photocatalytic Performance of Novel Electrospun BN/$TiO_2$ Composite Nanofibers. *New J. Chem.* **2017**, *41*, 81–89. [CrossRef]
15. Lee, C.-G.; Na, K.-H.; Kim, W.-T.; Park, D.-C.; Yang, W.-H.; Choi, W.-Y. $TiO_2$/ZnO Nanofibers Prepared by Electrospinning and Their Photocatalytic Degradation of Methylene Blue Compared with $TiO_2$ Nanofibers. *Appl. Sci.* **2019**, *9*, 3404. [CrossRef]
16. Park, S.-M.; Razzaq, A.; Park, Y.H.; Sorcar, S.; Park, Y.; Grimes, C.A.; In, S.-I. Hybrid $Cu_xO$–$TiO_2$ Heterostructured Composites for Photocatalytic $CO_2$ Reduction into Methane Using Solar Irradiation: Sunlight into Fuel. *ACS Omega* **2016**, *1*, 868–875. [CrossRef]
17. Sayegh, S.; Tanos, F.; Nada, A.; Lesage, G.; Zaviska, F.; Petit, E.; Rouessac, V.; Yatsunskiy, I.; Coy, E.; Viter, R.; et al. Tunable $TiO_2$-BN-Pd Nanofibers by Combining Electrospinning and Atomic Layer Deposition to Enhance Photodegradation of Acetaminophen. *Dalton Trans.* **2022**, *51*, 2674–2695. [CrossRef]
18. Cheng, X.; Yu, X.; Xing, Z.; Yang, L. Synthesis and Characterization of N-Doped $TiO_2$ and Its Enhanced Visible-Light Photocatalytic Activity. *Arab. J. Chem.* **2016**, *9*, S1706–S1711. [CrossRef]
19. Sudhakar, V.; Krishnamoorthy, K. Enhancing the Device Efficiency by Filling the Traps in Photoanodes. *J. Mater. Chem. C* **2019**, *7*, 14632–14638. [CrossRef]
20. Isari, A.A.; Hayati, F.; Kakavandi, B.; Rostami, M.; Motevassel, M.; Dehghanifard, E. N, Cu Co-Doped $TiO_2$@functionalized SWCNT Photocatalyst Coupled with Ultrasound and Visible-Light: An Effective Sono-Photocatalysis Process for Pharmaceutical Wastewaters Treatment. *Chem. Eng. J.* **2020**, *392*, 123685. [CrossRef]
21. Dong, F.; Wang, H.; Wu, Z.; Qiu, J. Marked Enhancement of Photocatalytic Activity and Photochemical Stability of N–Doped $TiO_2$ Nanocrystals by Fe3+/Fe2+ Surface Modification. *J. Colloid Interface Sci.* **2010**, *343*, 200–208. [CrossRef]
22. Huang, J.; Dou, L.; Li, J.; Zhong, J.; Li, M.; Wang, T. Excellent Visible Light Responsive Photocatalytic Behavior of N-Doped $TiO_2$ toward Decontamination of Organic Pollutants. *J. Hazard. Mater.* **2021**, *403*, 123857. [CrossRef]
23. Zhang, Z.; Wang, X.; Long, J.; Gu, Q.; Ding, Z.; Fu, X. Nitrogen-Doped Titanium Dioxide Visible Light Photocatalyst: Spectroscopic Identification of Photoactive Centers. *J. Catal.* **2010**, *276*, 201–214. [CrossRef]
24. Xing, M.; Zhang, J.; Chen, F. New Approaches to Prepare Nitrogen-Doped $TiO_2$ Photocatalysts and Study on Their Photocatalytic Activities in Visible Light. *Appl. Catal. B Environ.* **2009**, *89*, 563–569. [CrossRef]
25. Abid, M.; Sayegh, S.; Iatsunskyi, I.; Coy, E.; Lesage, G.; Ramanavicius, A.; Ben Haj Amara, A.; Bechelany, M. Design of Halloysite-Based Nanocomposites by Electrospinning for Water Treatment. *Colloids Surf. Physicochem. Eng. Asp.* **2022**, *651*, 129696. [CrossRef]
26. Abi Younes, P.; Sayegh, S.; Nada, A.A.; Weber, M.; Iatsunskyi, I.; Coy, E.; Abboud, N.; Bechelany, M. Elaboration of Porous Alumina Nanofibers by Electrospinning and Molecular Layer Deposition for Organic Pollutant Removal. *Colloids Surf. Physicochem. Eng. Asp.* **2021**, *628*, 127274. [CrossRef]
27. Kawrani, S.; Nada, A.A.; Bekheet, M.F.; Boulos, M.; Viter, R.; Roualdes, S.; Miele, P.; Cornu, D.; Bechelany, M. Enhancement of Calcium Copper Titanium Oxide Photoelectrochemical Performance Using Boron Nitride Nanosheets. *Chem. Eng. J.* **2020**, *389*, 124326. [CrossRef]
28. Martins, P.; Kappert, S.; Nga Le, H.; Sebastian, V.; Kühn, K.; Alves, M.; Pereira, L.; Cuniberti, G.; Melle-Franco, M.; Lanceros-Méndez, S. Enhanced Photocatalytic Activity of Au/$TiO_2$ Nanoparticles against Ciprofloxacin. *Catalysts* **2020**, *10*, 234. [CrossRef]
29. Nasr, M.; Balme, S.; Eid, C.; Habchi, R.; Miele, P.; Bechelany, M. Enhanced Visible-Light Photocatalytic Performance of Electrospun RGO/$TiO_2$ Composite Nanofibers. *J. Phys. Chem. C* **2017**, *121*, 261–269. [CrossRef]
30. Papoulis, D.; Komarneni, S.; Panagiotaras, D.; Stathatos, E.; Toli, D.; Christoforidis, K.C.; Fernández-García, M.; Li, H.; Yin, S.; Sato, T.; et al. Halloysite–$TiO_2$ Nanocomposites: Synthesis, Characterization and Photocatalytic Activity. *Appl. Catal. B Environ.* **2013**, *132–133*, 416–422. [CrossRef]
31. Danfá, S.; Martins, R.C.; Quina, M.J.; Gomes, J. Supported $TiO_2$ in Ceramic Materials for the Photocatalytic Degradation of Contaminants of Emerging Concern in Liquid Effluents: A Review. *Molecules* **2021**, *26*, 5363. [CrossRef] [PubMed]
32. Fischer, K.; Grimm, M.; Meyers, J.; Dietrich, C.; Gläser, R.; Schulze, A. Photoactive Microfiltration Membranes via Directed Synthesis of $TiO_2$ Nanoparticles on the Polymer Surface for Removal of Drugs from Water. *J. Membr. Sci.* **2015**, *478*, 49–57. [CrossRef]
33. Konstantinou, I. Photocatalytic Transformation of Pesticides in Aqueous Titanium Dioxide Suspensions Using Artificial and Solar Light: Intermediates and Degradation Pathways. *Appl. Catal. B Environ.* **2003**, *42*, 319–335. [CrossRef]

34. Sayegh, S.; Abid, M.; Tanos, F.; Cretin, M.; Lesage, G.; Zaviska, F.; Petit, E.; Navarra, B.; Iatsunskyi, I.; Coy, E.; et al. N-Doped $TiO_2$ Nanotubes Synthesized by Atomic Layer Deposition for Acetaminophen Degradation. *Colloids Surf. Physicochem. Eng. Asp.* **2022**, *655*, 130213. [CrossRef]
35. Addamo, M.; Bellardita, M.; Di Paola, A.; Palmisano, L. Preparation and Photoactivity of Nanostructured Anatase, Rutile and Brookite $TiO_2$ Thin Films. *Chem. Commun.* **2006**, 4943–4945. [CrossRef] [PubMed]
36. Bumajdad, A.; Madkour, M.; Abdel-Moneam, Y.; El-Kemary, M. Nanostructured Mesoporous Au/$TiO_2$ for Photocatalytic Degradation of a Textile Dye: The Effect of Size Similarity of the Deposited Au with That of $TiO_2$ Pores. *J. Mater. Sci.* **2014**, *49*, 1743–1754. [CrossRef]
37. Di Valentin, C.; Finazzi, E.; Pacchioni, G.; Selloni, A.; Livraghi, S.; Paganini, M.C.; Giamello, E. N-Doped $TiO_2$: Theory and Experiment. *Chem. Phys.* **2007**, *339*, 44–56. [CrossRef]
38. Sathishkumar, P.; Pugazhenthiran, N.; Mangalaraja, R.V.; Guesh, K.; Contreras, D.; Anandan, S. Contemporary Achievements of Visible Light-Driven Nanocatalysts for the Environmental Applications. In *Photocatalytic Functional Materials for Environmental Remediation*; John Wiley & Sons, Ltd.: Hoboken, NJ, USA, 2019; pp. 69–129. [CrossRef]
39. Chen, X.; Burda, C. Photoelectron Spectroscopic Investigation of Nitrogen-Doped Titania Nanoparticles. *J. Phys. Chem. B* **2004**, *108*, 15446–15449. [CrossRef]
40. Yu, Y.P.; Xing, X.J.; Xu, L.M.; Wu, S.X.; Li, S.W. N-Derived Signals in the X-ray Photoelectron Spectra of N-Doped Anatase $TiO_2$. *J. Appl. Phys.* **2009**, *105*, 123535. [CrossRef]
41. Yang, S.; Chen, G.; Lv, C.; Li, C.; Yin, N.; Yang, F.; Xue, L. Evolution of Nanopore Structure in Lacustrine Organic-Rich Shales during Thermal Maturation from Hydrous Pyrolysis, Minhe Basin, Northwest China. *Energy Explor. Exploit.* **2018**, *36*, 265–281. [CrossRef]
42. Jiang, L.; Huang, Y.; Liu, T. Enhanced Visible-Light Photocatalytic Performance of Electrospun Carbon-Doped $TiO_2$/Halloysite Nanotube Hybrid Nanofibers. *J. Colloid Interface Sci.* **2015**, *439*, 62–68. [CrossRef]
43. Vaiano, V.; Sannino, D.; Sacco, O. Heterogeneous Photocatalysis. In *Nanomaterials for the Detection and Removal of Wastewater Pollutants*; Elsevier: Amsterdam, The Netherlands, 2020; pp. 285–301. [CrossRef]
44. Cong, Y.; Zhang, J.; Chen, F.; Anpo, M. Synthesis and Characterization of Nitrogen-Doped $TiO_2$ Nanophotocatalyst with High Visible Light Activity. *J. Phys. Chem. C* **2007**, *111*, 6976–6982. [CrossRef]
45. Fang, J.; Wang, F.; Qian, K.; Bao, H.; Jiang, Z.; Huang, W. Bifunctional N-Doped Mesoporous $TiO_2$ Photocatalysts. *J. Phys. Chem. C* **2008**, *112*, 18150–18156. [CrossRef]
46. Divyasri, Y.V.; Lakshmana Reddy, N.; Lee, K.; Sakar, M.; Navakoteswara Rao, V.; Venkatramu, V.; Shankar, M.V.; Gangi Reddy, N.C. Optimization of N Doping in $TiO_2$ Nanotubes for the Enhanced Solar Light Mediated Photocatalytic $H_2$ Production and Dye Degradation. *Environ. Pollut.* **2021**, *269*, 116170. [CrossRef] [PubMed]
47. Jadhav, P.S.; Jadhav, T.; Bhosale, M.; Jadhav, C.H.; Pawar, V.C. Structural and Optical Properties of N-Doped $TiO_2$ Nanomaterials. *Mater. Today Proc.* **2021**, *43*, 2763–2767. [CrossRef]
48. Noorisepehr, M.; Kakavandi, B.; Isari, A.A.; Ghanbari, F.; Dehghanifard, E.; Ghomi, N.; Kamrani, F. Sulfate Radical-Based Oxidative Degradation of Acetaminophen over an Efficient Hybrid System: Peroxydisulfate Decomposed by Ferroferric Oxide Nanocatalyst Anchored on Activated Carbon and UV Light. *Sep. Purif. Technol.* **2020**, *250*, 116950. [CrossRef]
49. Gómez-Avilés, A.; Peñas-Garzón, M.; Bedia, J.; Rodriguez, J.J.; Belver, C. C-Modified $TiO_2$ Using Lignin as Carbon Precursor for the Solar Photocatalytic Degradation of Acetaminophen. *Chem. Eng. J.* **2019**, *358*, 1574–1582. [CrossRef]
50. Konstantinou, I.K.; Albanis, T.A. $TiO_2$-Assisted Photocatalytic Degradation of Azo Dyes in Aqueous Solution: Kinetic and Mechanistic Investigations. *Appl. Catal. B Environ.* **2004**, *49*, 1–14. [CrossRef]
51. Le, T.X.H.; Nguyen, T.V.; Amadou Yacouba, Z.; Zoungrana, L.; Avril, F.; Nguyen, D.L.; Petit, E.; Mendret, J.; Bonniol, V.; Bechelany, M.; et al. Correlation between Degradation Pathway and Toxicity of Acetaminophen and Its By-Products by Using the Electro-Fenton Process in Aqueous Media. *Chemosphere* **2017**, *172*, 1–9. [CrossRef]